Applied Catalysis B: Environmental 187 (2016) 238–248

Contents lists available at ScienceDirect

Applied Catalysis B: Environmental

journal homepage: www.elsevier.com/locate/apcatb

Low-temperature active, oscillation-free PdNi(alloy)/Ni-foam catalyst with enhanced heat transfer for coalbed methane deoxygenation via catalytic combustion

Qiaofei Zhang, Yakun Li, Ruijuan Chai, Guofeng Zhao *, Ye Liu, Yong Lu *

Shanghai Key Laboratory of Green Chemistry and Chemical Processes, School of Chemistry and Molecular Engineering, East China Normal University, Shanghai 200062, China

ARTICLE INFO

Article history:
Received 30 October 2015
Received in revised form
23 December 2015
Accepted 17 January 2016
Available online 21 January 2016

Keywords:
Structured catalyst
Coalbed methane
PdNi alloy
Ni foam
Catalytic combustion

ABSTRACT

A high-performance PdNi(alloy)/Ni-foam catalyst to be used for coalbed methane (CBM) deoxygenation via catalytic combustion was developed with the aid of galvanic deposition of Pd nanoparticles onto the monolithic Ni-foam followed by in-situ reaction-induced Pd-Ni alloying. The investigations concerning the preparation/reaction conditions and heat/mass transfer indicated that such PdNi(alloy)/Ni-foam catalyst provided a unique combination of high low-temperature activity/selectivity, oscillation-free, high permeability and enhanced heat transfer. As an example, the catalyst with a low Pd-loading of 1 wt% could deliver a complete O_2 conversion for a simulated feed of $CH_4/O_2/N_2$ (40/3/57, vol%) at 350 °C with a high gas hourly space velocity of 12,000 mL $g_{cat.}^{-1}$ h^{-1}, and particularly, this catalyst was stable for at least 500 h without deactivation and reaction oscillation. In-situ reaction-induced Pd-Ni alloying was clearly revealed and by nature was responsible for the low-temperature activity (expressed by turnover frequency) promotion and oscillation suppression. The underlying mechanism for CBM deoxygenation over the PdNi(alloy)/Ni-foam catalyst is proposed to be a Langmuir-Hinshelwood type.

1. Introduction

Concerns about the severe dilemma between the fast growing energy demand and the depletion of conventional energy resources such as petroleum have been spurring worldwide impetus to explore the non-conventional energy resources. Coalbed methane (CBM), also known as coal mine gas or coal seam gas, is one kind of flammable gas whose major component is methane (CH_4), and possesses huge world's reserves of about 1200 trillion cubic feet [1]. Its effective utilization as a reliable alternative energy resource will not only help to fill the supply-demand gap of natural gas, but also reduce its own air pollution because CH_4 is 21 times more effective than carbon dioxide as a greenhouse gas [1]. The CBM released before, during and after mining operations possesses the CH_4 concentration of 60–95%, 30–90%, and 0.1–1.0%, respectively. The part of CBM with 60–95% CH_4 concentration is easy to use, but the rest with lower CH_4 concentration is directly discharged into the atmosphere or utilized as a low-energy-fuel gas in local heat-generating plants or thermal-electric power stations. Particularly, the part of CBM with 30–90% CH_4 concentration is usually mixed with some amount of O_2 and its content is in the explosive range (3–15%). In this context, O_2 removal for this part of oxygen-bearing CBM is imperative to meet the transportation requirement through natural gas pipeline (with O_2 molar content of below 0.1%) for a high-value-added utilization, but greatly challenging because of the risk of explosion during O_2-removal process [2].

Catalytic combustion is a qualified method for, according to different CH_4 concentration, O_2 removal (namely CBM deoxygenation with high CH_4 concentration of above 30% and low O_2 concentration of below 10%) and CH_4 removal (namely demethane with contrastively low CH_4 concentration of 1.0–0.1% and high O_2 concentration of above 15%) [3–5], and the essence of both processes is catalytic combustion of the extremely inert

Abbreviations: CBM, coalbed methane; SCRs, structured catalysts and reactors; SNG, synthetic natural gas; PPI, pores per inch; CFD, computational fluid dynamics; ICP-AES, inductively coupled plasma atomic emission spectroscopy; SEM, scanning electron microscopy; BSE, back-scattering electron; EDX, energy dispersive X-ray fluoresence spectrometer; TEM, transmission electron microscopy; HRTEM, high-resolution transmission electron microscopy; SSA, specific surface area; BET, Brunauer-Emmett-Teller; XRD, X-ray diffraction; XPS, X-ray photoelectron spectroscopy; H_2-TPR, H_2-temperature programmed reduction; TCD, thermal conductivity detector; TGA, thermogravimetric analysis; GHSV, gas hourly space velocity; GC, gas chromatography; TOF, turnover frequency; PD, pressure drop; 3D, three-dimensional; BE, binding energy; DFT, density functional theory.

* Corresponding authors.
E-mail address: ylu@chem.ecnu.edu.cn (Y. Lu).

http://dx.doi.org/10.1016/j.apcatb.2016.01.041
0926-3373/

Nomenclature

ΔH_{298}	Molar enthalpy of reaction at 298 K (kJ mol^{-1})
2θ	Bragg-diffraction angle (○)
V_m	Molar volume of gas (L mol^{-1})
F	O_2 flow (L s^{-1})
α	Yield of CO_2
N	Number of active sites (mol g^{-1})

CH_4 with O_2 (*i.e.*, $CH_4 + 2O_2 = CO_2 + 2H_2O$) associated with a huge ΔH_{298} of −802.7 kJ mol^{-1}. Undisputedly, high catalyst activity for catalytic CH_4 combustion is the primarily considered issue to ensure its low-temperature competence. More extensive studies are currently focused on the catalytic CH_4 combustion for the de-methane process rather than the CBM deoxygenation. Various single and mixed metal oxides (such as CoO_x with preferentially exposed optimum planes and mixed-oxides with favorably tuned properties) have been commonly investigated because of their cost-effectiveness but suffer from high light-off temperature [6–10]. Oxides-supported noble metals (such as Pt, Rh and Pd) with strong metal-oxide interactions are generally preferred for catalytic CH_4 combustion by virtue of their high low-temperature activity, low light-off temperature and good poison resistance [11,12]. Especially for Pd-based catalysts, extensive studies are focused on the relationship between the activity and chemical state of Pd, as well as Pd-support interactions. PdO_x is generally considered to be critical to this reaction [11,12], but unfortunately, PdO_x tends to deactivate by sintering or by transformation into metallic Pd at >600 °C. According to the understanding of the stabilizing-effect on PdO_x originated from oxides-Pd interactions [13], modular Pd@CeO_2 [11] and Pd@ZrO_2 [12] core-shell complexes were designed to enhance Pd-oxide interactions and indeed achieved the enhanced activity and stability. For the CBM deoxygenation process, the investigations are rather limited, but a similar tendency still shows that the noble-metal catalysts are more active than the oxide catalysts [10,14]. Under the CH_4-rich condition, CBM deoxygenation will show a disparate kinetic model due to the reaction kinetics depends strongly on the partial pressure of reactants [4,8,10,15], thereby some different catalytic behaviors may be found during the investigation of CBM deoxygenation.

Despite of the above advances in improving the catalyst activity, oscillatory behavior that the reaction rate oscillates along with reaction time and temperature [16–18], is commonly present for the CBM deoxygenation especially on Pd-based catalysts [19,20], which is not expected. Furthermore, the practical applications of oxide-supported Pd catalysts remain another great challenge because the conventional randomly packed bed technology is ill-suited for this strongly exothermic reaction and high-throughput process on account of poor catalyst heat conductivity and high pressure drop [21]. For example, removing 10% O_2 will consume 5% CH_4, and the bed temperature may reach 1000 °C or above (adiabatic temperature rise is at least 700 °C) [14]. Therefore, to meet the requirements of rapid dissipation of huge reaction heat and high throughput operation for such catalytic CBM deoxygenation process, exploration on novel catalyst and/or catalytic reactor technology is particularly desirable, aiming at the integration of high catalytic-performance (high activity, selectivity and stability, and oscillation suppression) with significantly enhanced heat/mass transfer.

Recently, structured catalysts and reactors (SCRs) have received ever-increasing attention in the process integration and intensification for the industrial catalysis and environment protection [22–26]. Such new approaches provide unique combination of low pressure drop, easy recycling operation, modular reactor design, and especially controllable mass and heat transfer ability, making them superior to randomly packed bed reactors with conventional pellet catalysts [27]. As previously reported, various microfibrous-structured catalysts have been successfully developed and demonstrated in wide applications especially for the strong exothermic/endothermic reactions with enhanced catalytic performance and heat transfer, including alcohol selective oxidation, hydrogenolysis of dimethyl oxalate to ethylene glycol, Fischer-Tropsch synthesis, dry reforming of CH_4, and portable H_2 production via ammonia cracking and methanol steam reforming [28–35]. The open-cell metallic foams are also considered as prospective candidates for structured catalyst development, because of their characteristic of interconnected open cells which leads to low pressure drop and facilitates gas/solid heat/mass transfer [36–39]. However, their practical applications in catalysis are greatly restricted because cost-effective and highly efficient preparation of foam-structured catalysts is still a challenging area. Conventional washcoating techniques for the catalytic functionalization face the risks of nonuniformity and exfoliation of the coatings as well as the binder contamination [40,41]. Most recently, monolithic foam-based catalysts for the strongly exothermic reactions such as syngas methanation for synthetic natural gas (SNG) production and catalytic oxy-methane reforming, were developed by the modified wet chemical etching of Ni-foam, providing unique combination of high activity/selectivity, excellent stability and enhanced heat transfer [42–44].

In present work, we discovered a high-performance monolithic PdNi(alloy)/Ni-foam catalyst for the catalytic CBM deoxygenation and demonstrated its facile fabrication engineered from micro- to macro-scales via galvanic exchange reaction deposition (called "galvanic deposition" hereafter) method [28–32,34,35] followed by in-situ reaction-induced Pd-Ni alloying in the real reaction stream. The effects of the catalyst preparation and reaction conditions on the catalyst performance were investigated, as well as its permeability and heat conductivity, the oscillatory behavior at different temperatures, and the stability. These experiment results indicated that this new approach provided a combination of enhanced heat transfer, desired mechanical robustness, and excellent low-temperature activity/selectivity and reaction stability with oscillation suppression in the CBM deoxygenation process via catalytic combustion. Moreover, the characterization results clearly identified the formation of PdNi alloy on the Ni-foam and the formed PdNi alloy was contributed to the low-temperature activity and oscillation suppression.

2. Experimental

2.1. Catalyst preparation

The catalyst was prepared with the aid of galvanic exchange reaction between Ni-foam and palladium (or palladium-containing) ions, followed by washing thoroughly with deionized water, drying at 100 °C overnight and calcining at 450 °C for 2 h in air. Ni-foam chips (100 PPI, 2 mm thickness, and 8.0 mm diameter; purchased from Changsha Lyrun Material Co., Ltd, China) were obtained from their large parent sheets by laser cutting. Palladium was anchored onto the Ni-foam struts by the galvanic deposition, which could proceed spontaneously at room temperature once Ni-foam chips were impregnated with palladium salt aqueous solutions (such as $Pd(NO_3)_2$, $Pd(Ac)_2$, $PdCl_2$, K_2PdCl_6 and $(NH_4)_2PdCl_6$ dissolved in deionized water), owing to the large electrode potential differences between the Ni^{2+}/Ni° (−0.26 V) and Pd^{2+}/Pd° (0.95 V) or $PdCl_6^{2-}/Pd^{\circ}$ (1.91 V) pairs. The pre-made solution of each palladium salt was fixed at a concentration of 0.05 g Pd per gram. For example, $Pd(NO_3)_2$ solution of 0.20 g

(0.001 g Pd) was weighted for preparing the catalyst with nominal Pd loading of 1 wt%, which was diluted to 5 mL and subsequently used to impregnating 1.00 g Ni-foam chips. Prior to the galvanic deposition, Ni-foam chips were cleaned by immersing them in a diluted aqueous solution of nitric acid (1 wt% HNO_3) at room temperature for removing the NiO film originally existing on the Ni-foam struts.

To compare the heat transfer between our monolithic catalyst and conventional particulate catalyst in computational fluid dynamics (CFD) simulation, we prepared a reference catalyst of Pd/SiO_2 (1 wt% Pd) using incipient wetness impregnation method with $Pd(NO_3)_2$ as precursor and 0.2 mm SiO_2 as support (Alfa Aesar, surface area of 89 $m^2\,g^{-1}$), followed by drying at 100 °C overnight and calcining at 450 °C for 2 h.

2.2. Catalyst characterization

The actual loading of Pd was determined by dissolving the samples in aqua regia solution and measuring the Pd ion concentration by inductively coupled plasma atomic emission spectroscopy (ICP-AES; ICP Thermo IRIS Intrepid II XSP; USA). The scanning electron microscopy (SEM) and back-scattering electron (BSE) images were obtained on Hitachi S-4800 microscopy equipped with an energy dispersive X-ray fluoresence spectrometer (EDX, Oxford; UK). The catalysts were also characterized by transmission electron microscopy (TEM, FEI-Tecnai G2F30) operating at 300 kV.

Specific surface area (SSA) was determined using standard Brunauer-Emmett-Teller (BET) theory based on N_2 adsorption isotherms obtained at −196 °C on a Quantachrome Autosorb-3B instrument. X-ray diffraction (XRD) patterns were obtained by a Rigaku Ultra IV diffractometer using Cu Kα radiation at 35 kV and 25 mA in the 2θ scanning range of 5–90° and scanning rate of 60° min^{-1}. The X-ray photoelectron spectroscopy (XPS) was recorded on an Escalab 250xi spectrometer, using a standard Al Kα X-ray source (300 W) and an analyzer pass energy of 20 eV. All binding energies were referenced to the adventitious C1s line at 284.8 eV.

H_2-temperature programmed reduction (H_2-TPR) and CO pulse adsorption were performed on a Quantachrome ChemBET-3000 chemisorption apparatus with a thermal conductivity detector (TCD) and an online mass spectrometer (Proline Dycor, AMETEK Process Instrument, USA). Typically, 100 mg of catalyst was loaded into a quartz tube with quartz wool at both sides. For H_2-TPR, samples were pretreated in He flow at 300 °C for 1 h and then cooled down to 20 °C. After that, the gas mixture of 10% H_2 in N_2 was fed into the tube with a total flux of 50 mL min^{-1} and the sample was heated up to 600 °C with the ramp of 10 °C min^{-1}. The number of surface Pd sites per unit mass of catalyst was determined by CO pulse adsorption at 20 °C after the following pretreatments and assuming the adsorption stoichiometry of CO/Pd = 1:1 [45,46]. The samples were pretreated in He flow at 300 °C for 1 h and then reduced at 150 °C in a gas mixture of 10% H_2 in N_2. In order to exclude the competitive CO adsorption on Ni-foam, a reference catalyst of Ni-foam which was treated by the dilute nitric acid (1 mol L^{-1}) followed by calcination at 450 °C for 2 h was prepared. After reduction at 480 °C in a gas mixture of 10% H_2 in N_2, the CO pulse adsorption was performed over the referenced Ni-foam and the result showed that a small amount of CO (1.5×10^{-7} mol g^{-1}) was adsorbed. Therefore, the amount of adsorbed CO on the catalysts was excluded the amount of adsorbed CO on Ni atoms.

Thermogravimetric analysis (TGA) curves of the used catalysts were performed on a Simultaneous TG-DTA/DSC Apparatus (High Temperature Platform 400, STA 449 F3 Jupiter, NETZSCH-Gerätebau GmbH) from 25 to 900 °C in an air flow of 80 mL min^{-1} at a heating rate of 10 °C min^{-1}, to determine the total amount of carbon deposition.

2.3. Reactivity tests

The catalytic CBM deoxygenation was performed on a fixed-bed quartz tube reactor (600 mm length by 8 mm inner diameter) under atmospheric pressure. A gaseous mixture of $CH_4/O_2/N_2$ (40/3/57, vol%) was employed as feedstock and gas hourly space velocity (GHSV) was set to 12000 mL g^{-1} h^{-1}, if not specified. Circular chips (8.0 mm diameter) of the foam-structured Pd catalyst were packed layer-up-layer into the tube reactor. The weight of each catalyst chip is about 0.022 g and eleven pieces of chips with the overall dosage of 0.25 g were used for reactivity tests. Notice that a little larger diameter of the catalyst chips than the inner diameter of the tubular reactor was deliberately retained to avoid the appearance of a gap between the reactor wall and the edges of catalyst chips, thereby preventing gas bypass. Three calibrated mass flow controllers were used to control the flow velocity of CH_4, oxygen and nitrogen gas. The thermocouple (outer diameter: 0.5 mm) for temperature measurement was inserted into the catalyst chips very easily, because the catalyst has an extendable three-dimensional network and large void volume. Given that the hot spots generally appeared in the upper layer of the catalyst bed, the temperatures at the midpoint of upper catalyst bed were measured, and the temperature differences from reactor wall to the upper layer of the catalyst bed were identified as the temperature-rising of hot spots. The product effluent was analyzed online by an HP 6850 gas chromatography (GC) equipped with TCD connected to Porapak Q and MS 5A parallel capillary columns (DIKMA). The gas pipeline and sampling 6-way valve between the reactor outlet and the GC injector were heated to ensure the effluent completely evaporated. Each point of the conversion curves was sampled after undergoing reaction under the stationary condition for 0.5 h. The catalyst activity was defined by T_{10}, T_{50} and T_{90}, representing the reaction temperatures for the oxygen conversion of 10%, 50% and 90%, respectively.

2.4. TOF calculation

In order to assess the intrinsic activity, so called turnover frequency (TOF, here defined as the quantity of CO_2 produced per surface Pd atom per hour) was calculated. The quantity of CO_2 formed per unit time (mol s^{-1}) could be obtained by dividing the molar volume of gas (V_m, L mol^{-1}, assuming ideal behavior at 25 °C) into the flow of O_2 (F, L s^{-1}) times α (the yield of CO_2). The number (N, mol g^{-1}) of active sites (*i.e.*, surface Pd atoms) was determined by CO pulse chemisorption. In accordance, the TOF could be calculated by:

$$\mathrm{TOF} = \frac{\mathrm{ProductMolecules}}{\mathrm{ActiveSites} \times \mathrm{Time}} = \frac{\mathrm{F} \times \alpha}{\mathrm{V_m} \times \mathrm{N}}$$

The data for TOF calculation was evaluated in a plug flow reactor for laboratory use. In order to eliminate transport limitations, large gas velocity and small catalyst particle size were employed. For the monolithic catalyst, if the catalyst layer is thinner than 8 μm, the internal mass transfer resistance would be eliminated [47]. Low conversion at moderate reaction temperature can eliminate temperature gradient and external mass transfer resistance. So the O_2 conversion for CBM deoxygenation was retained at below 10% by tuning the GHSV at 280 °C. As an example, the TOF of PdNi(alloy)/Ni-foam was calculated as following. The flow of O_2 gas (F) was set to 10.0 mL min^{-1}. At 280 °C, about 7.95% of O_2 was converted into CO_2 product over 0.15 g catalyst with 100% CO_2 selectivity for a feedgas of $CH_4/O_2/N_2$ (40/3/57, vol%) at total GHSV of 134000 mL g^{-1} h^{-1}, and thus the yield of CO_2 (*i.e.*, α) accounted to 3.98%. The molar amount of surface Pd per gram our

representative PdNi(alloy)/Ni-foam catalyst was determined to be 2.2×10^{-5} mol g^{-1} by CO chemisorption. It was supposed that every surface Pd atom was an active site, the TOF of PdNi(alloy)/Ni-foam could thus be calculated as:

$$\mathrm{TOF} = \frac{\frac{10}{1000\times 60}(\mathrm{Ls}^{-1}) \times 0.0398}{240.8(\mathrm{Lmol}) \times 22 \times 10^{-5}(\mathrm{molg}^{-1}) \times 0.15(\mathrm{g})} = 00.081\mathrm{s}^{-1} = 292\mathrm{h}^{-1}$$

2.5. Pressure drop determination

The pressure drop (PD) through our PdNi(alloy)/Ni-foam bed and particulate Pd/SiO_2 packed bed was measured by the method reported in our previous work [48]. PD measurement was performed by using a sample cell consisting of an 8 mm (inner diameter) tube fitting with 5 mm (inner diameter) transparent plastic tube inserted into the ends of the fitting. The cell with two O-ring rubber gaskets at front and back was equipped with spacers inside the fitting to hold the sample properly. The catalyst dosage was 0.25 g and the gas flow was well controlled by a mass flow controller. The PD was measured by a Magnehelica 2000-250 PA differential pressure gauge (Dwyer, USA) at various values of the inlet flow rate of nitrogen.

2.6. CFD calculation

The temperature distribution at steady state inside the catalytic bed (inner diameter, 8.0 mm) was obtained by the finite-volume based commercial CFD code FLUENT, version 6.3.26. The tubular reactor was divided into three parts and the middle part where catalyst placed was set isothermal. The catalytic bed contacting to the isothermal wall was initially set at a uniform temperature of 350 °C. In the simulation of CBM deoxygenation, the PdNi(alloy)/Ni-foam catalyst (bed voidage of 95%; Table S1) and the reference particulate catalyst of Pd/SiO_2 (nominal Pd-loading of 1 wt%, SiO_2 support of 0.2 mm, and bed voidage of 35%; Table S1) were packed in the quartz tubular reactor with catalyst dosage of 0.25 g, respectively. Almost equivalent O_2 conversions of 95 ~ 100% were obtained over both Ni-foam-structured and SiO_2-supported Pd catalysts at 350 °C for the mixture feedgas of $CH_4/O_2/N_2$ (40/3/57, vol%) with flow rate of 50 mL min^{-1}, and therefore, equivalent amount of reaction heat was released from both catalyst surfaces. The model was shown in Fig. S1 and the simulation methods were described in the Supporting Information and Fig. S2.

3. Results and discussion

3.1. Ni-foam-structured Pd catalysts engineered from micro- to macro-scales via facile galvanic deposition method

Common Ni-foam with three-dimensional (3D) continuously open-cell structure (Fig. S3) was employed as the monolithic substrate. Boosted by the galvanic exchange reaction between Ni-foam and palladium salts (such as $Pd(NO_3)_2$, $Pd(Ac)_2$, $PdCl_2$, K_2PdCl_6 and $(NH_4)_2PdCl_6$ dissolved in deionized water) and subsequent calcination in air, fresh Ni-foam-structured Pd catalysts were obtained. Note that such galvanic deposition process proceeded spontaneously once Ni-foam was wetted by an aqueous palladium salt solution to appointed nominal Pd-loading of 1 wt%, because of the large electrode potential differences between Pd^{2+}/Pd° (or Pd^{4+}/Pd°) and Ni^{2+}/Ni° pairs. The actual Pd-loading was determined to be 0.9 wt% by ICP-AES, indicating the high efficiency of this galvanic deposition method. Fig. 1 shows the geometry, morphology and microstructure features of our representative as-prepared catalyst using palladium nitrate precursor. As shown in Fig. 1A and B, the fresh catalyst showed well-preserved monolithic structure, and its textural features were characteristic of 100 PPI, voidage volume of 95 vol%, and cell window size of 150–300 μm. The SSA was increased from 3.9 m^2 g^{-1} of the Ni-foam substrate to 7.9 m^2 g^{-1} of the fresh catalyst after calcining at 450 °C (Table 1). Table S2 also showed that the fresh catalysts obtained after calcining at temperature ranged from 300 to 600 °C all delivered almost equal SSA (7.3–8.1 m^2 g^{-1}). Besides the dominant nickel phase from the unreacted foam struts, as evidenced by XRD patterns in Fig. 1C, clear Pd phase was also observed in the fresh catalyst as well as minor NiO and PdO phases. SEM/EDX line scanning and mapping images clearly showed that the formed Pd, PdO and NiO uniformly self-assembled into burr-like particles, which covered across the foam-strut surface (Figs. 1D -G and S4). The BSE image showed many bright spots around with amorphous structure, while high-resolution TEM image showed a special ensemble of a Pd nanoparticle partially covered with tiny NiO (Fig. 1H and I). Accordingly, the fresh Ni-foam-structured Pd catalyst is referred as to Pd-PdO-NiO/Ni-foam.

3.2. Effects of activation, preparation parameters and reaction conditions

3.2.1. In-situ reaction activation

The above-mentioned freshly-prepared Pd-PdO-NiO/Ni-foam catalyst was directly examined in the catalytic CBM deoxygenation using a feedgas of $CH_4/O_2/N_2$ (40/3/57, vol%) at a GHSV of 12,000 mL g^{-1} h^{-1}. As shown in Fig. 2A and Table 1, along with the increase of temperature, O_2 conversion increased from 3.1% at 280 °C continuously to 10% at 305 °C (T_{10}), 50% at 330 °C (T_{50}) and then up to 90% at 340 °C (T_{90}). With further increasing temperature, O_2 conversion could reach 100% at 350 °C, but surprisingly, underwent a valley with temperature from 360 to 430 °C; until to 440 °C, complete O_2 conversion was achieved again at or above this temperature (Fig. 2A). Specifically, the O_2 conversion was monitored with time-on-stream at 380 °C, and it was interestingly found that the O_2 conversion did not remain constant at 42%, but exhibited an obvious oscillation behavior that O_2 conversion fluctuated up and down over the reaction time (Fig. 2B).

After undergoing the reaction at 480 °C for 1 h (named as in-situ reaction activation), the catalyst was tested again with the decrease of reaction temperature from 480 to 220 °C and then with the increase from 220 to 450 °C (Fig. 2). Notably, the formation of PdNi alloy occurred definitely associated with such in-situ reaction activation, solidly evidenced by XRD analyses combined with XPS measurements (detailed discussion in posterior Section 3.5). The in-situ activated catalyst is thus named as PdNi(alloy)/Ni-foam. Interestingly, over the PdNi(alloy)/Ni-foam catalyst the temperature for the same O_2 conversion was lowered by 30–40 °C compared to the fresh Pd–PdO-NiO/Ni-foam (for example, T_{90} decreased from 340 °C for the Pd-PdO-NiO/Ni-foam to 308 °C for the PdNi(alloy)/Ni-foam, Fig. 2A and Table 1). More interestingly, our PdNi(alloy)/Ni-foam catalyst could suppress oscillation when the reaction temperature cooled down and ran up under identical reaction conditions (Fig. 2). The above results clearly indicated that the in-situ reaction-induced activation not only improved the low-temperature catalytic activity but also endowed the catalyst with oscillation-suppression property. Therefore, the reaction results reported in the posterior parts are all based on the in-situ activated catalysts, unless otherwise specified.

3.2.2. Pd precursor, calcination temperature and Pd-loading

Various palladium salts with different valence of Pd ions were used as precursors to prepare the monolithic Ni-foam structured Pd catalysts via the galvanic deposition method, and the precursor-effect on their CBM deoxygenation performance was initially investigated at appointed Pd-loading of 1 wt%. As shown in Fig. S5A

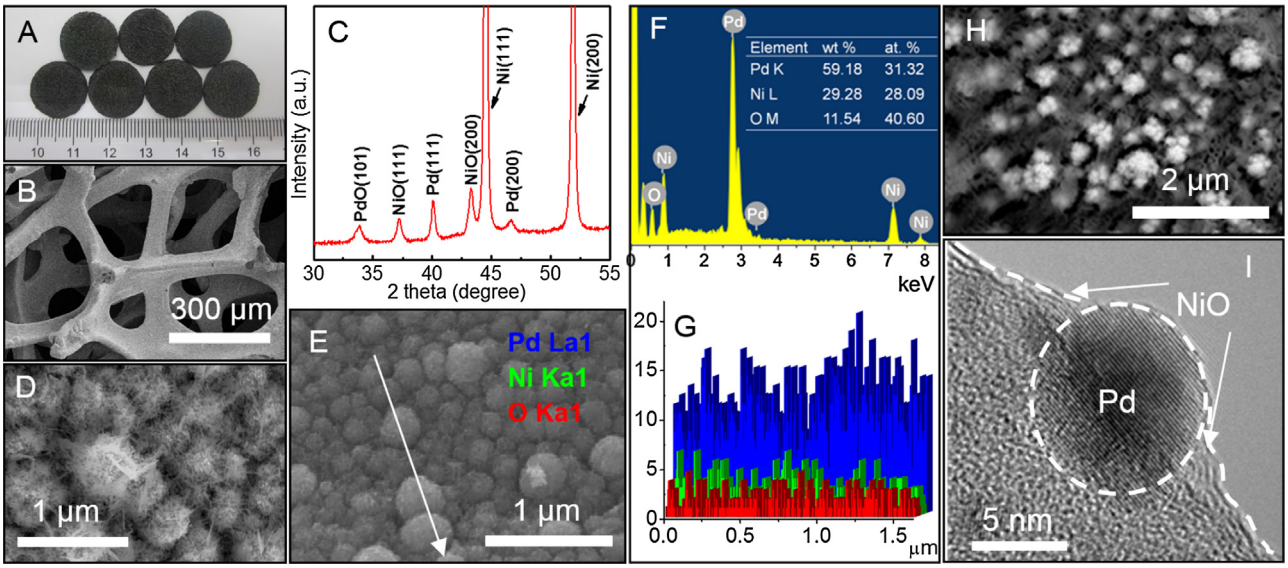

Fig. 1. Structural features from macro- to micro-scales of the fresh Pd-PdO-NiO/Ni-foam sample (1 wt% Pd): (A) photograph, (B) low-magnitude SEM image, (C) XRD pattern, (D) high-magnitude SEM image, (E–G) SEM-EDX line scanning images, (H) BSE image and (I) TEM image.

Table 1
CBM deoxygenation catalyzed by the Pd-PdO-NiO/Ni-foam catalyst before and after in-situ activation.

Catalyst	Pd loading[a] (wt%)	S_{BET} ($m^2\ g^{-1}$)	T_{10} (°C)	T_{50} (°C)	T_{90}[b] (°C)	Surf. Pd[c] (mol g^{-1})	TOF[d] (h^{-1})
Fresh	0.9	7.9	305	330	340	4.0×10^{-6}	57
Activated	0.9	27.4	258	295	308	2.2×10^{-5}	292

[a] Measured by ICP-AES.
[b] T_{10}, T_{50} and T_{90} represent the reaction temperatures for the oxygen conversion of 10%, 50% and 90%, respectively (0.25 g Cat., $CH_4/O_2/N_2$ = 40/3/57 (vol%), GHSV = 12,000 mL g_{cat}^{-1} h^{-1}.
[c] Determined by CO pulse absorption.
[d] Turnover frequency at 280 °C (TOF, h^{-1}) based on CO_2 yield and surface Pd.

and Table S3, the reaction results clearly showed an inconspicuous variation in activity over the catalysts obtained using different palladium precursors. For example, the catalysts prepared from K_2PdCl_4 and $PdCl_2$ delivered the T_{50} of 309 and 290 °C respectively, and their T_{50} difference was only 19 °C. Moreover, their comparable TOFs were varied in a range from 270 to 312 h^{-1}, ranking in an order that was consistent with the O_2 conversions against the Pd precursors. Based on the overall consideration of both cost and catalytic performance, the most common palladium nitrate seemed a cost-efficient Pd catalyst precursor.

Subsequently, the effect of calcination temperature on the catalyst performance for this reaction was investigated over the Ni-foam structured Pd (1 wt%) catalysts obtained using palladium nitrate precursor, with the results as shown in Fig. S5B. Clearly, the catalyst activity for the CBM deoxygenation was dependent on the calcination temperature. The T_{10}, T_{50} and T_{90} decreased with the calcination temperature from 300 to 450 °C but then increased while further increasing the calcination temperature from 450 to 600 °C. The best catalyst was the one after calcining at 450 °C, with obvious oscillation-suppression (Fig. 2B), being highly active with a very low T_{90} of 308 °C for a feed of $CH_4/O_2/N_2$ (40/3/57, vol%) using a high GHSV of 12000 mL $g_{cat.}^{-1}$ h^{-1}. More notably, in addition to the deteriorated activity, calcining at high temperature of 500 °C or above resulted in serious reaction oscillation (Fig. S6). Such exorbitant calcination temperature facilitated the formation of excessive NiO species thereby severely covering the Pd

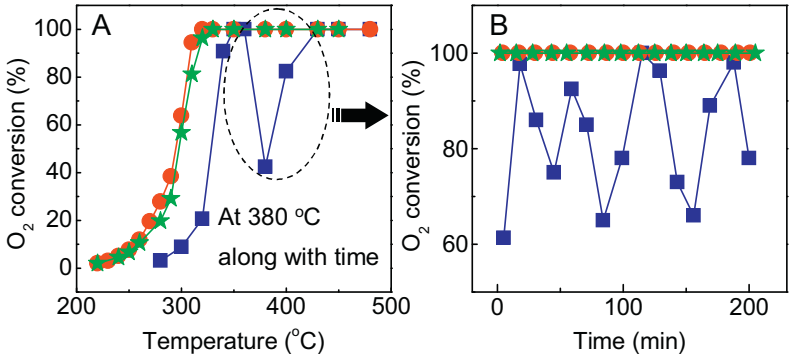

Fig. 2. (A) O_2 conversion for catalytic CBM deoxygenation against reaction temperature and (B) O_2 conversion at 380 °C *vs* time on stream. Note: (■: Path 1) Temperature increasing from 280 to 480 °C; (●: Path 2) After undergoing reaction at 480 °C for 1 h, temperature from 480 to 220 °C; (★: Path 3) After Path 2, temperature increasing from 220 to 450 °C. Reaction conditions: 0.25 g Cat., $CH_4/O_2/N_2$ of 40/3/57 (vol%), GHSV of 12,000 mL $g_{cat.}^{-1}$ h^{-1}.

nanoparticles (NPs), which was detrimental to the in-situ reaction-induced Pd-Ni alloying (corresponding to the improvement of low-temperature activity and oscillation suppression, discussed in posterior Section 3.5). Not surprisingly, because no in-situ reaction-induced PdNi alloying happened on the catalyst samples after calcining at and above 500 °C, their TOFs were comparable to that ($57\ h^{-1}$) for the fresh Pd-PdO-NiO/Ni-foam catalyst (Table S2). In addition, the particle size of PdNi alloy was increased very slightly with the calcination temperature up to 450 °C, while such sintering became a little bit obvious after calcining at and above 500 °C. Table S2 also showed that the in-situ activated catalysts all provided comparable SSA (21.6 to $27.4\ m^2\ g^{-1}$), which were almost 2 times higher compared to the fresh ones (7.3 to $8.1\ m^2\ g^{-1}$). This observation might be contributed to both the reconstruction of the catalyst layer firmly embedded onto the Ni-foam struts and the formation of some carbon during the in-situ reaction activation at 480 °C. This was tentatively confirmed by the SEM morphology change before (Fig. 1D) and after activation (Fig. S7), and carbon deposit of 0.5 ~ 0.7 wt% determined by TGA results. When the carbon deposit was removed by calcination at 500 °C in air, SSA of the activated samples was decreased to $\sim 10\ m^2\ g^{-1}$, indicating that their SSA increment mainly originated from carbon deposit. Moreover, the catalyst layer of the in-situ activated one showed a mesoporous feature with an average pore diameter of approximately 45 nm (Fig. S8).

The effect of Pd-loading was also investigated to check how low the palladium usage could be at desirable reactivity. What to be noted is that the actual Pd-loadings of all the catalyst samples were almost identical to be ~90% of the corresponding nominal loadings (Table S4), and the nominal Pd-loadings were used in discussion. The catalysts with nominal Pd-loadings varied from 0.5 to 3.0 wt% all showed monotonically increasing indicative of the activity with the reaction temperature, but interestingly, not with the Pd-loading. The highest activity was observed at a Pd-loading of 2 wt% for a feed of $CH_4/O_2/N_2$ (40/3/57, vol%) using a high GHSV of $12{,}000\ mL\ g_{cat.}^{-1}\ h^{-1}$ (Fig. S5C). For instance, with varying the Pd-loading from 0.5 to 3 wt%, the catalysts successively delivered T_{90} of 348 °C (0.5 wt% Pd), 308 °C (1 wt% Pd), 300 °C (2 wt% Pd), and 304 °C (3 wt% Pd). Reasonably, the Pd-loading of 1 wt% well balanced the catalyst cost with the catalytic performance. It was found that with the increase of Pd-loading, surface Pd amount scaled linearly but the activity of the catalyst with the highest Pd-loading was not the highest. Meanwhile, TOF of the 3 wt% Pd-loading catalyst with large particle size (6 nm) was lower than the other ones with small particle size (3–4 nm, Table S4). This demonstrated that the influence of Pd-loading on the activity for CBM deoxygenation over the PdNi(alloy)/Ni-foam was intrinsically an effect of PdNi alloy particle size.

Based on above results, the best Ni-foam-structured Pd catalyst obtained by galvanic deposition method was the one with Pd-loading of 1 wt% after calcining at 450 °C in air and subsequent in-situ reaction-induced activation (*i.e.*, undergoing reaction at a higher reaction temperature (*e.g.*, 480 °C) for 1 h; Fig. 2 and Table 1). Therefore, the introduction of Pd by the galvanic deposition method for catalytic functionalization of Ni-foam remarkably improved the low-temperature activity and suppressed the oscillation.

3.2.3. Reaction conditions

The effects of reaction conditions, including GHSV, CH_4 concentration and O_2 concentration, on the performance of our PdNi(alloy)/Ni-foam (Pd: 1 wt%) catalyst for the CBM deoxygenation via catalytic CH_4 combustion were also investigated with results as shown in Fig. 3. The GHSV effect was firstly investigated, and the results in Fig. 3A showed that, with the increase of GHSV from 9000 to $72{,}000\ mL\ g^{-1}\ h^{-1}$, T_{10} smoothly increased from 248 to 272 °C, as did T_{50} and T_{90}. Clearly, low space velocity facilitated O_2 conversion because of a long contact time of reactants with catalyst bed. It should be noted that complete O_2 conversion cannot be reachable once the GHSV was over $72{,}000\ mL\ g^{-1}\ h^{-1}$ even at 480 °C in this study.

Considering the changeable concentration of CH_4 and O_2 in the practical CBM deoxygenation, the effects of CH_4 and O_2 concentrations on O_2 conversion were subsequently investigated. The general pattern of catalytic combustion of CH_4 has been well established [49]: As temperature increasing, oxidation is initiated at a temperature that depends on the nature of catalyst (initial stage); a further increase of temperature leads to an exponential increase in O_2 conversion until O_2 is depleted (like Fig. 2A). Accordingly, the effects of CH_4 and O_2 concentrations were studied at the initial stage (*i.e.*, at the reaction temperatures of 280 and 300 °C) with the results shown in Fig. 3B and C. Increasing CH_4 concentration could increase the O_2 conversion while increasing O_2 concentration contrarily led to the decrease of O_2 conversion.

3.3. High permeability and heat conductivity

As previously stated, the excellent permeability and heat conductivity are other important specialties of a catalyst required for the high-throughput and strongly exothermic reaction processes, which are particularly pronounced in the CBM deoxygenation via catalytic CH_4 combustion. As expected, the studies based on permeability-measurement experiment and CFD simulation showed much lower pressure drop and temperature rising of our PdNi(alloy)/Ni-foam catalyst bed than the conventional particulate catalyst packed bed, indicating the higher permeability and heat transfer of our monolithic-structured catalyst.

Fig. S9 shows the benefit of higher permeability of the foam-structured catalyst bed compared with the particulate Pd/SiO_2 catalyst packed bed. Not surprisingly, the PD increased linearly in both foam-structured bed and particulate packed bed with gas velocity in the range studied but much slower for the former than the later. Our Ni-foam-structured catalyst bed with 95 vol% voidage exhibited much lower PD than particulate Pd/SiO_2 catalyst (0.2 mm) bed: $15\ kPa\ m^{-1}$ *vs* $220\ kPa\ m^{-1}$ at a N_2 superficial velocity of $0.3\ m\ s^{-1}$. Even at a very high superficial velocity of $0.85\ m\ s^{-1}$, our foam-structured catalyst bed produced a slightly increased PD of only $33\ kPa\ m^{-1}$, less than a tenth of that ($400\ kPa\ m^{-1}$) for the Pd/SiO_2 packed bed at a low superficial velocity of $0.55\ m\ s^{-1}$.

Fig. S10 shows the steady-state temperature distributions within the two catalyst beds, and it is clearly that hot spots appeared in the upwind-side of the reactor bed where the reaction took place intensively in both reactors. Not surprisingly, the particulate Pd/SiO_2 catalyst bed generated a hot spot with ~290 °C temperature-rising because of its poor heat transfer. In contrast, our Ni-foam-structured Pd catalyst bed generated a hot spot with much lower temperature-rising of only ~70 °C, as a result of its enhanced heat transfer [28–30,33]. Furthermore, as shown in Fig. 2A, O_2 conversions for cooling (reaction temperature decreased from 480 to 220 °C) and heating (reaction temperature increased from 220 to 450 °C) curves at each reaction temperature set point were very close over the in-situ activated catalyst. This observation indicated that trapping the reaction heat in the temperature-cooling process which undoubtedly made a higher O_2 conversion otherwise was avoided as a result of high thermal conductivity of our foam-structured catalyst.

3.4. Stability

Long-term test was carried out over the in-situ activated catalyst for a feedgas of $CH_4/O_2/N_2$ (40/3/57, vol%) using a GHSV of $12{,}000\ mL\ g^{-1}\ h^{-1}$. The catalyst could stably afford a complete O_2 conversion at 350 °C for 230 h without any signs of fluctuation

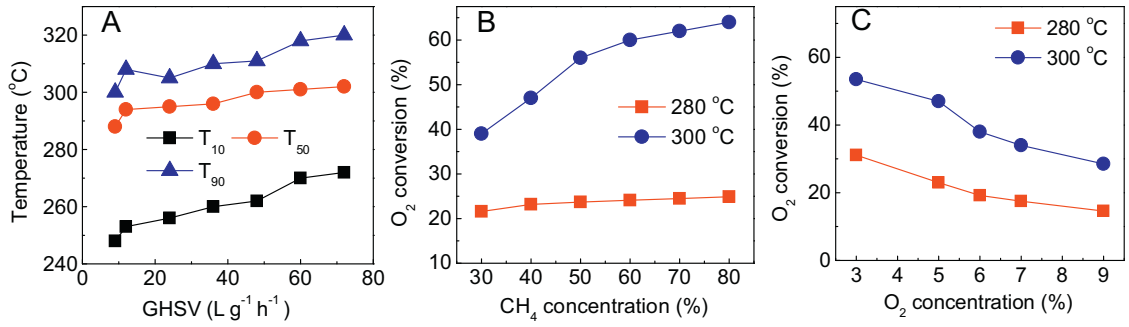

Fig. 3. Effects of reaction conditions on the performance of the in-situ activated catalyst for CBM deoxygenation: (A) GHSV with $CH_4/O_2/N_2$ of 40/3/57 (vol%), (B) CH_4 concentration with GHSV of 12,000 mL $g_{cat.}^{-1}$ h^{-1} and constant O_2 concentration of 3% and (C) O_2 concentration with GHSV of 12,000 mL $g_{cat.}^{-1}$ h^{-1} and constant CH_4 concentration of 40%.

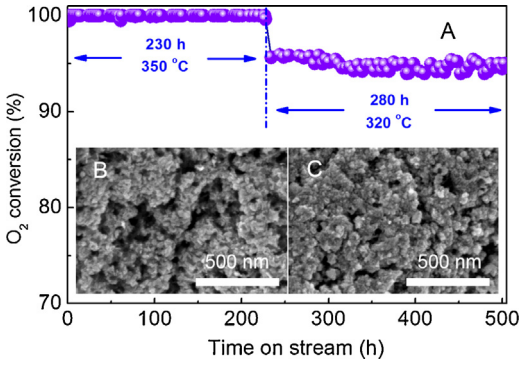

Fig. 4. (A) O_2 conversion for CBM deoxygenation *vs* time on stream using the in-situ activated PdNi(alloy)/Ni-foam catalyst (1 wt% Pd). Reaction conditions: 0.25 g Cat., $CH_4/O_2/N_2$ of 40/3/57 (vol%), GHSV of 12,000 mL $g_{cat.}^{-1}$ h^{-1}. SEM images of the activated PdNi(alloy)/Ni-foam: (B) after 1 h activation and (C) after 510 h on stream.

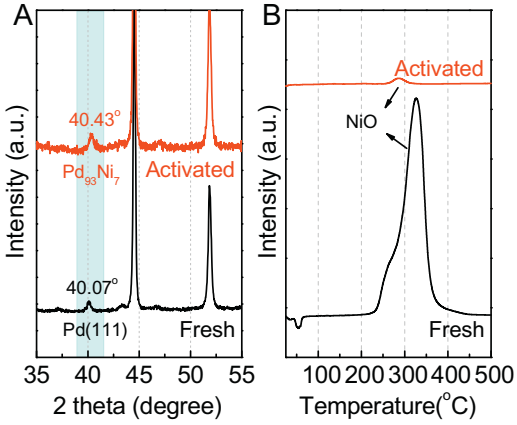

Fig. 5. XRD patterns (A) and H_2-TPR profiles (B) for the fresh Pd-PdO-NiO/Ni-foam (undergoing reaction at 350 °C) and activated PdNi(alloy)/Ni-foam (in situ activated at 480 °C) catalysts. The H_2-TPR results showed that NiO was reduced during the in-situ reaction activation process. Note that the negative peaks of H_2-TPR profile for the fresh catalyst at below 100 °C were attributed to hydrogen desorption from the bulk Pd nanoparticles.

(Fig. 4A). In order to avoid the illusion of the long lifetime caused by the excess of catalyst, an incomplete O_2 conversion of ~95% was sustained for another 280 h at 320 °C, and no signs of oscillation and deactivation were shown either. Not surprisingly, the in-situ activated catalyst undergoing 510-h test showed the almost unchanged XRD phase peak of PdNi alloy (Fig. S11) and well-preserved surface structure compared to the initial form of the catalyst (Fig. 4B and C), indicating the promising robustness of our catalyst for this strongly exothermal combustion reaction.

3.5. Pd-Ni alloying: the essence of activity improvement and oscillation elimination

3.5.1. Activity improvement

The catalytic performance of the Pd–PdO-NiO/Ni-foam catalyst was dramatically improved after the in-situ reaction activation at 480 °C for 1 h (Fig. 2A). For a reference, the pristine Ni-foam was also tested and showed poor activity for the CBM deoxygenation, delivering a limited O_2 conversion of only 31% even at 480 °C (Fig. S12). Now the question we have to naturally ask is what happened to the catalyst during the in-situ reaction activation process. To seek the answer, CO chemisorption was firstly carried out to probe the catalyst surface with the results as shown in Table 1. Interestingly, in-situ reaction activation resulted in a 4-fold increase of the amount of surface Pd compared to the fresh catalyst: 2.2×10^{-5} mol g^{-1} *vs* 4.0×10^{-6} mol g^{-1}. More interestingly, such activation process provided a 4-fold improvement of the intrinsic activity expressed by the TOF: 292 h^{-1} for the activated *vs* 57 h^{-1} for the fresh. Based on these preliminary results, it is rational to infer that there is a specific surface reconfiguration associated with the in-situ reaction activation.

To reveal the nature of such activation-promotion observation, both the fresh and in-situ activated catalysts were characterized by XRD and H_2-TPR (Fig. 5). Clearly, weak NiO and faint PdO XRD peaks that were detectable on the fresh catalyst disappeared on the catalyst after in-situ reaction activation at 480 °C, and meanwhile, the dominant Pd(1 1 1) XRD peak shifted from 40.07° to 40.43°. The above observation undoubtedly indicated that NiO as well as PdO was reduced during the in-situ reaction activation process and Ni atoms diffused into Pd NPs to form PdNi alloy, in which Ni content was estimated to be 7 at% according to the Vegard's law [50]. In addition, HRTEM results also confirmed the formation of PdNi alloy with a lattice spacing of 0.215 nm, which was between the characteristics of face-centered cubic Pd (0.224 nm) and Ni (0.203 nm) crystal phase in the (1 1 1) facet, and a narrow size distribution with average PdNi alloy nanoparticle size of 3.7 nm (Fig. S13), being consistent with the size estimated by Scherrer equation (4.0 nm).

The PdNi alloy formation was further confirmed by the XPS results. After in-situ reaction activation, the $Pd3d_{5/2}$ binding energy (BE) was up-shifted from 335.1 eV for the fresh catalyst to 335.9 eV (Fig. 6A), which was ascribed to the changes of valence electron density and matrix shift of Pd atoms resulted from Ni diffusion into Pd NPs [51,52]. Moreover, the Ni2p spectra showed the almost disappearance of nickel oxide (Ni2p BE of 853.7 eV) on the in-situ activated catalyst (Fig. 6B). Associated with the activation, meanwhile, the catalyst surface was transformed from Ni-rich to Pd-rich with Pd/Ni atom ratio increased from 0.1 to 1.6 (Table 2) due to the lower surface free energy of Pd [53,54], which was in good agree-

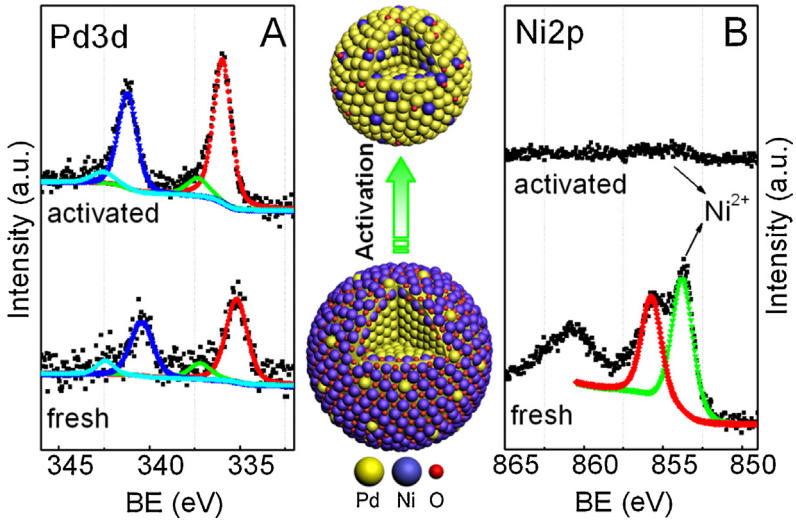

Fig. 6. XPS spectra in (A) Pd3d and (B) Ni2p regions of the Pd-PdO-NiO/Ni-foam catalyst after reaction at 350 °C and the in-situ activated one after reaction at 480 °C for 1 h. The scheme in the middle shows the evolution from Pd-PdO-NiO to PdNi alloy during the in-situ activation process.

Table 2
XPS analysis of Pd-PdO-NiO/Ni-foam and PdNi(alloy)/Ni-foam catalyst[a].

Sample	$Pd3d_{5/2}$ (eV)		Pd^0/Pd^{2+} (atom)	$Ni2p_{3/2}$ (eV)	Pd/Ni (atom)
	Pd^0	Pd^{2+}			
Fresh[b]	335.1	337.2	5.0	853.7	0.1
Activated[c]	335.9	337.3	6.4	853.7	1.6
Activated-used[d]	335.9	337.2	5.7	853.9	1.4

[a] Pd^0: metallic Pd. Pd^{2+}: Pd oxide.
[b] The freshly obtained Pd-PdO-NiO/Ni-foam catalyst undergoing reaction at 400 °C.
[c] After in-situ reaction activation at 480 °C.
[d] The activated PdNi(alloy)/Ni-foam catalyst undergoing reaction at 400 °C.

ment with the CO chemisorption results (Table 1). By combining the information of Pd-Ni alloying with the fact of activation-improved activity, it is rational for us to believe that PdNi alloy formation was responsible for the 4-fold increase of the intrinsic activity. The Pd-Ni alloying during the in-situ reaction activation is schematically illustrated in Fig. 6 and the resulting catalyst is thus expressed as PdNi(alloy)/Ni-foam. Notably, traces of PdO and NiO were still detectable on the PdNi(alloy)/Ni-foam catalyst surface by XPS combined with H_2-TPR (Figs. 5B and 6), mostly being assignable to the intermediate species generated in the oxidation-reduction (redox) cycles for catalytic combustion of CH_4 [8,11,49].

3.5.2. Calcination temperature-dependence of Pd-Ni alloying

As shown in Table S2, the observed activity improvement stemmed from in-situ reaction activation was dependent on the calcination temperature of fresh catalyst, likely indicating that the Pd-Ni alloying evolution would be sensitive to the catalyst calcination temperature. To clearly clarify this observation, the Pd-Ni alloying evolution of the catalysts calcined at various temperatures before and after in-situ reaction activation was tracked using XRD and H_2-TPR (Fig. 7). Clearly, the amounts of NiO and PdO on the fresh catalysts were progressively increased with the calcination temperature, especially at and above 500 °C. After in-situ reaction activation, only on the catalysts calcined at below 500 °C, the formed NiO and PdO species could be reduced completely accompanied with the formation of PdNi alloy (*i.e.*, Pd(111) shifting toward higher diffraction angle); on the contrary, large amount of NiO still existed and no PdNi alloy phase was formed over those catalysts calcined at and above 500 °C. Combining the above information with the fact that the catalysts calcined at <500 °C delivered much higher intrinsic activity than the other ones calcined at >500 °C, it is now safe to say that the Pd-Ni alloying was essential to the activity improvement and oscillation-suppression. The exorbitant calcination temperatures resulted in excessive NiO formation that heavily covered the Pd NPs. This might be the main cause for hindering the formation of PdNi alloy thereby leading to poor catalyst activity.

3.5.3. Oscillation suppression

Many catalytic reactions exhibit oscillatory behavior that reaction rate spontaneously oscillates as a function of reaction time and temperature, and it is also a common behavior in CBM deoxygenation (namely in the CH_4-rich atmosphere) especially for Pd catalysts [14–18,55], which is generally originated from the redox cycles composed of the stepwise O_2-adsorption/activation and elimination of oxygen species by CH_4 [17–20,55,56]. Similarly, our fresh Pd-PdO-NiO/Ni-foam catalyst also presented such undesirable oscillation phenomenon. A weakened oscillatory behavior over Pd/Al_2O_3 modified by CeO_2 was reported, which reflected some stabilization of a chemical state of the Pd active phase during reaction, due to the capabilities of CeO_2 for oxygen storage [57]. Notably, our PdNi(alloy)/Ni-foam catalyst could entirely suppress oscillation when the reaction temperature ran up and cooled down for a feedgas of $CH_4/O_2/N_2$ (40/3/57, vol%) using a GHSV of 12,000 mL g^{-1} h^{-1} (Fig. 2). We believed that in-situ formation of PdNi alloy was paramount to such oscillation suppression. A possible explanation is that the Pd-Ni alloying helps to balance the stepwise O_2-adsorption/activation and elimination of oxygen species by CH_4 [56] thereby leading to the suppression of oscillation.

To further clarify the PdNi-alloy-related oscillation suppression, a series of control-experiments on the fresh Pd-PdO-NiO/Ni-foam and activated PdNi(alloy)/Ni-foam catalysts were carried out. As shown in Fig. 8A, the fresh catalyst showed oscillatory behavior in a wide reaction temperature range from 350 to 430 °C for a feedgas of $CH_4/O_2/N_2$ (40/3/57, vol%) at 12,000 mL g^{-1} h^{-1}. The fresh catalyst samples after reaction at and below 410 °C showed H_2-TPR profiles almost same as that for the sample without undergoing reaction, and not surprisingly, reaction oscillation occurred over all those samples with considerable fluctuation in O_2 conversion against time on stream. Notably, the oscillation started to be weakened on the fresh samples when running the reaction at 420 °C and completely disappeared when increasing the reaction tem-

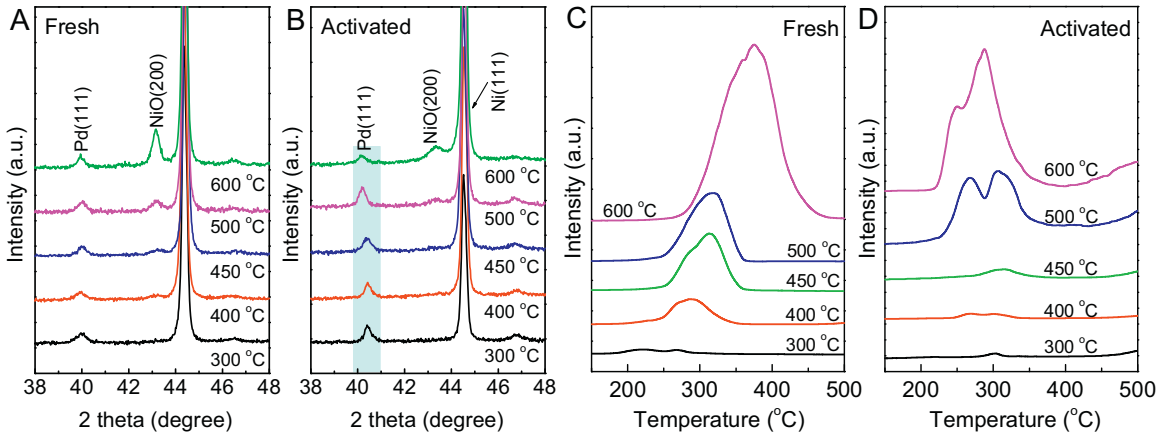

Fig. 7. (A,B) XRD patterns and (C,D) H_2-TPR profiles for catalysts calcining at different temperatures: (A,C) fresh Pd-PdO-NiO/Ni-foam and (B,D) PdNi(alloy)/Ni-foam undergoing reaction at 400 °C.

perature up to 440 °C. For the sample after reaction at 420 °C, a low-temperature shoulder peak appeared on its H_2-TPR profile, likely indicating the start of Pd-Ni alloying which in turn catalyzed the reduction of NiO. Along with increasing reaction temperature to and above 430 °C, the H_2-TPR peak of the corresponding catalyst samples showed a fading tendency similar with the reaction oscillation while Pd-Ni alloying proceeded (Figs. 8A and S14). In addition, the PdNi(alloy)/Ni-foam (*i.e.*, in-situ activated at 480 °C for 1 h) demonstrated excellent oscillation-suppression maintenance in a wide reaction temperature range from 480 to 330 °C. As expected, the catalyst surface state remained almost unchanged evidenced by PdNi alloy phase maintenance with the presence of trace NiO species at the temperatures studied (Figs. 8B and S14). For the catalytic CH_4 combustion under CH_4-rich condition, the reaction paths involve the redox cycle composed of O_2-oxidation and CH_4-reduction of the catalyst. Over the Pd catalyst, the adsorption and dissociation of oxygen is faster than CH_4, and it is difficult for their chemisorption to match each other well [58,59] thereby leading to oxygen self-poisoning and consequent oscillation [60]. Our foregoing results clearly revealed that PdNi alloy showed ability to significantly suppress the oscillation to a great extent in comparison with Pd alone, it is thus proposed that the stepwise redox cycles on Pd catalysts was transformed to be balanced transiently on the PdNi alloy catalyst, thus leading to the suppression of oscillation [56].

3.5.4. *Preliminary discussion of the mechanism for CBM deoxygenation*

Mars-van-Krevelen mechanism involving Pd-PdO_x cycles has been recognized as a commonly accepted one for lean methane combustion over the Pd-based catalysts [61,62]. In particular, PdO_x (*i.e.*, lattice oxygen) plays a major role in CH_4 oxidation activity. Under oxygen-rich condition the surface of Pd-based catalysts is covered with O_2 (based on thermodynamics principle) and thus the oxidation of methane is independent of O_2 concentration. However, reaction kinetics depends strongly on the partial pressure of reactants [4]. Therefore, CBM deoxygenation will show a disparate reaction mechanism.

In terms of our previously reported DFT calculation results for CBM deoxygenation [56], O_2 adsorption is more facile at Pd(111) and the adsorbed O atoms (O*) adsorb more strongly at Pd(111) than at PdNi(111). The activation barrier of methane is 0.85 eV at clean Pd(111) and 1.14 eV at PdNi(111). However, with pre-adsorbed O at different sites, methane dissociation would be

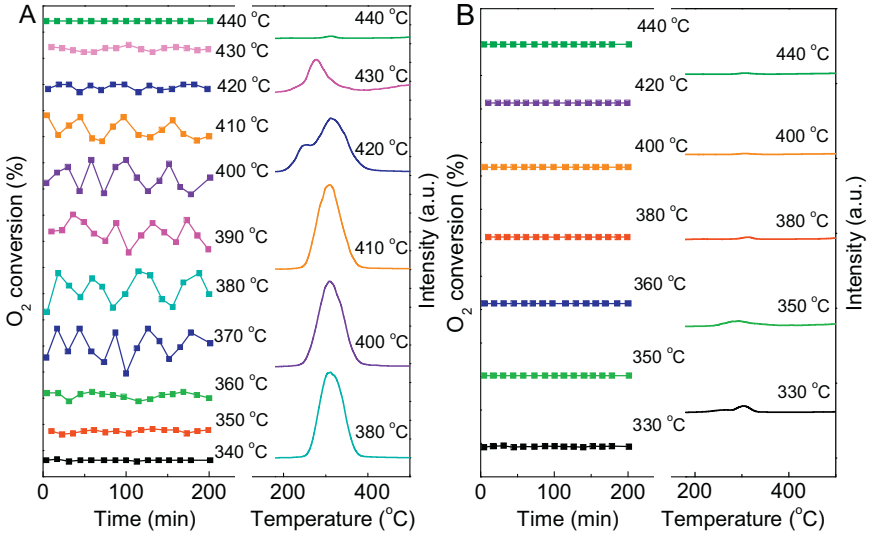

Fig. 8. Oscillatory behavior on O_2 conversion for CBM deoxygenation and the corresponding H_2-TPR profiles over the Ni-foam structured catalysts. (A) The fresh Pd-PdO-NiO/Ni-foam, and (B) the activated PdNi(alloy)/Ni-foam. Reaction conditions: 0.25 g Cat., $CH_4/O_2/N_2$ of 40/3/57 (vol%), GHSV of 12,000 mL $g_{cat.}^{-1}$ h^{-1}.

suppressed significantly at Pd(111). Therefore, the strong adsorption of O* at Pd(111) is unfavorable to methane activation, which will then significantly decrease the O_2 conversion rate until the excessive surface adsorbed O atoms are consumed, inducing an oscillatory behavior over the fresh catalyst. Interestingly, the adsorbed species like O_2* and O* are preferably targeted by H* at PdNi(111). Thus fast O_2 conversion by H* at PdNi(111) can effectively decrease the surface coverage of O*, which is beneficial to methane activation and avoiding the oscillatory behavior caused by accumulated surface adsorbed O*. We infer that the capability of direct O_2*/O* hydrogenation at PdNi(111) shifts the original cycles composed of stepwise O_2-adsorption/activation and oxidation-of-CH_4 at a Pd catalyst to the present transient-balancing cycles at our PdNi alloy catalyst thereby eliminating the oscillation. At the same time, the facile diffusion of O, favorable intermediates and the low energy barriers for the difficult steps of CH* and CO* oxidation by O* at PdNi(111) can further accelerate the O_2 elimination.

For catalytic oxidation reactions over the metal-based catalyst, the strength of metal-O bond plays a primary role in the catalytic performance. During the de-methane process, O* has strong affinity with Pd atoms over the Pd-based catalysts, leading to the formation of PdO_x (*i.e.*, lattice oxygen). Fujimoto et al. have shown that methane oxidation turnover rates depended strongly on the strength of Pd-O bonds and the density of oxygen-deficient PdO_x species [61]. Strong Pd-O bonds in small PdO_x crystallites and in oxygen-deficient PdO_x would lead to the decrease in TOFs, as the crystallite size decreased or as the crystallites became oxygen deficient when samples were treated at temperatures above those required for PdO-to-Pd decomposition. However, both the lattice oxygen and strong adsorbed O* are detrimental to the activity-enhancement and oscillation-suppression for CBM deoxygenation. For PdNi alloy, the charge transfer from Ni atoms to surface Pd atoms weakens the electron affinities between O* and Pd atoms, promoting the O* species to react with CH* and H* species. Therefore, the Langmuir-Hinshelwood mechanism is more suitable for PdNi alloy rather than the Mars-van-Krevelen mechanism.

4. Conclusions

A monolithic PdNi(alloy)/Ni-foam catalyst was tailored for the CBM deoxygenation via catalytic CH_4 combustion, which was obtained through galvanically depositing Pd NPs on a Ni-foam surface followed by in-situ reaction activation (*e.g.*, undergoing reaction at 480 °C for 1 h). Such galvanic deposition method was working highly effectively and efficiently to embed Pd onto the Ni-foam strut and not sensitive to the palladium salt precursors. The PdNi(alloy)/Ni-foam catalysts provided unique combination of high low-temperature activity/selectivity, good stability, oscillation suppression, low pressure drop at high-throughput operation, enhanced heat transfer and low Pd usage. For example, over the catalyst with a Pd-loading of 1 wt%, complete conversion of O_2 could be achieved and maintained for a simulated feed of $CH_4/O_2/N_2$ (40/3/57, vol%) at 350 °C with a high GHSV of 12,000 mL $g_{cat.}^{-1}$ h^{-1}. This foam-structured PdNi alloy catalyst was stable for at least 500 h without reaction oscillation and activity deterioration. Our experimental studies unanimously revealed that the in-situ reaction-induced Pd-Ni alloying contributed to the enhanced low-temperature activity/selectivity, promising stability and oscillation suppression. We anticipate our assay to be a new point for the CBM deoxygenation in both catalyst and O_2-lean catalytic CH_4 combustion chemistry, which might stimulate commercial exploitation of the new-generation structured catalyst technology toward CBM efficient utilization and environmental protection.

Acknowledgments

This work was financially supported by the "973 program" (2011CB201403) from the MOST of China, and the NSF of China (21473057, 21273075, U1462129).

Appendix A. Supplementary data

Supplementary data associated with this article can be found, in the online version, at http://dx.doi.org/10.1016/j.apcatb.2016.01.041.

References

[1] S. Su, J. Agnew, Fuel 85 (2006) 1201–1210.
[2] A. Olajossy, A. Gawdzik, Z. Budner, J. Dula, Chem. Eng. Res. Des. 81 (2003) 474–482.
[3] C.Ö. Karacan, F.A. Ruiz, M. Cotè, S. Phipps, Int. J. Coal Geol. 86 (2011) 121–156.
[4] F. Ortloff, J. Bohnau, F. Graf, T. Kolb, Appl. Catal. B 182 (2016) 375–384.
[5] F. Ortloff, J. Bohnaua, U. Kramarb, F. Graf, T. Kolb, Appl. Catal. B 182 (2016) 550–561.
[6] L. Hu, Q. Peng, Y. Li, J. Am. Chem. Soc. 130 (2008) 16136–16137.
[7] L.F. Liotta, H. Wu, G. Pantaleo, A.M. Venezia, Catal. Sci. Technol. 3 (2013) 3085–3102.
[8] T. Choudhary, S. Banerjee, V. Choudhary, Appl. Catal. A 234 (2002) 1–23.
[9] C.Y. Ma, Z. Mu, J.J. Li, Y.G. Jin, J. Cheng, G.Q. Lu, Z.P. Hao, S.Z. Qiao, J. Am. Chem. Soc. 132 (2010) 2608–2613.
[10] Z.C. Liu, G.Z. Lu, Y. Guo, Y.Q. Wang, Y.L. Guo, Catal. Sci. Technol. 1 (2011) 1006–1012.
[11] M. Cargnello, J.J.D. Jaén, J.C.H. Garrido, K. Bakhmutsky, T. Montini, J.J.C. Gámez, R.J. Gorte, P. Fornasiero, Science 337 (2012) 713–717.
[12] C. Chen, Y.-H. Yeh, M. Cargnello, C.B. Murray, P. Fornasiero, R.J. Gorte, ACS Catal. 4 (2014) 3902–3909.
[13] S. Colussi, A. Gayen, M.F. Camellone, M. Boaro, J. Llorca, S. Fabris, A. Trovarelli, Angew. Chem. Int. Ed. 48 (2009) 8481–8484.
[14] S.D. Wang, S. Wang, Z.S. Yuan, C.X. Zhang, C.J. Ni, D.Y. Li, US Patent 20120003132 A1 (2012).
[15] P. Gélin, M. Primet, Appl. Catal. B 39 (2002) 1–37.
[16] M. Slinko, V. Korchak, N. Peskov, Appl. Catal. A 303 (2006) 258–267.
[17] S. Vendelbo, C. Elkjær, H. Falsig, I. Puspitasari, P. Dona, L. Mele, B. Morana, B. Nelissen, R. van Rijn, J. Creemer, P. Kooyman, S. Helveg, Nat. Mater. 13 (2014) 884–890.
[18] S.J.A. Figueroa, M.A. Newton, J. Catal. 312 (2014) 69–77.
[19] V.Y. Bychkov, Y.P. Tyulenin, A.Y. Gorenberg, S. Sokolov, V.N. Korchak, Appl. Catal. A 485 (2014) 1–9.
[20] V.Y. Bychkov, Y.P. Tyulenin, M. Slinko, D.P. Shashkin, V.N. Korchak, J. Catal. 267 (2009) 181–187.
[21] A.J. Zarur, J.Y. Ying, Nature 403 (2000) 65–67.
[22] F.M. Dautzenberg, Catal. Rev. 46 (2004) 335–368.
[23] J. Gascon, J.R. van Ommen, J.A. Moulijn, F. Kapteijn, Catal. Sci. Technol. 5 (2015) 807–817.
[24] X. Wang, M. Wen, C. Wang, J. Ding, Y. Sun, Y. Liu, Y. Lu, Chem. Commun. 50 (2014) 6343–6345.
[25] G. Zhao, M. Deng, Y. Jiang, H. Hu, J. Huang, Y. Lu, J. Catal. 301 (2013) 46–53.
[26] J. Mao, M. Deng, L. Chen, Y. Liu, Y. Lu, AIChE J. 56 (2010) 1545–1556.
[27] E. Reichelt, M.P. Heddrich, M. Jahn, A. Michaelis, Appl. Catal. A 476 (2014) 78–90.
[28] G.F. Zhao, H.Y. Hu, M.M. Deng, Y. Lu, Chem. Commun. 47 (2011) 9642–9644.
[29] G.F. Zhao, Y.K. Li, Q.F. Zhang, M.M. Deng, F.H. Cao, Y. Lu, AIChE J. 60 (2014) 1045–1053.
[30] Q.F. Zhang, Y.K. Li, L. Zhang, L. Chen, Y. Liu, Y. Lu, J. Catal. 317 (2014) 54–61.
[31] L. Zhang, L.P. Han, G.F. Zhao, R.J. Chai, Q.F. Zhang, Y. Liu, Y. Lu, Chem. Commun. 51 (2015) 10547–10550.
[32] L. Han, C. Wang, G. Zhao, Y. Liu, Y. Lu, AIChE J. (2016), http://dx.doi.org/10.1002/aic.15061.
[33] W. Chen, W.Q. Sheng, G.F. Zhao, F.H. Cao, Q.S. Xue, L. Chen, Y. Lu, RSC Adv. 2 (2012) 3651–3653.
[34] M.M. Wang, J.F. Li, L. Chen, Y. Lu, Int. J. Hydrog. Energy 34 (2009) 1710–1716.
[35] M. Ling, G.F. Zhao, W. Chen, M.M. Wang, Q.S. Xue, Y. Lu, Int. J. Hydrog. Energy 36 (2011) 12833–12842.
[36] A. Montebelli, C.G. Visconti, G. Groppi, E. Tronconi, C. Cristiani, C. Ferreira, S. Kohler, Catal. Sci. Technol. 4 (2014) 2846–2870.
[37] H. Dai, B. Lin, Energy Fuels 28 (2014) 6644–6654.
[38] P.S. Roy, A.S. Raju, K. Kim, Fuel 139 (2015) 314–320.
[39] A. Alamdari, J. Nat. Gas Sci. Eng. (2016), http://dx.doi.org/10.1016/j.jngse.2015.09.037.
[40] Z. Ren, V. Botu, S.B. Wang, Y.T. Meng, W.Q. Song, Y.B. Guo, R. Ramprasad, S.L. Suib, P.X. Gao, Angew. Chem. Int. Ed. 53 (2014) 7223–7227.
[41] J. Sun, Y. Li, X. Liu, Q. Yang, J. Liu, X. Sun, D.G. Evans, X. Duan, Chem. Commun. 48 (2012) 3379–3381.
[42] Y.K. Li, Q.F. Zhang, R.J. Chai, G.F. Zhao, Y. Liu, Y. Lu, ChemCatChem 7 (2015) 1427–1431.

[43] Y.K. Li, Q.F. Zhang, R.J. Chai, G.F. Zhao, Y. Liu, Y. Lu, F.H. Cao, AIChE J. 61 (2015) 4323–4331.
[44] R. Chai, Y. Li, Q. Zhang, G. Zhao, Y. Liu, Y. Lu, Catal. Commun. 70 (2015) 1–5.
[45] T. Hattori, H. Matsumoto, Y. Murakami, Preparation of Catalysts IV, Elsevier, 1987, pp. 815, Uchijima.
[46] J.Y. Li, L. Ma, X.N. Li, C.S. Lu, H.Z. Liu, Ind. Eng. Chem. Res. 44 (2005) 5478–5482.
[47] H. Chen, H. Yu, Y. Tang, M. Pan, F. Peng, H. Wang, J. Yang, Appl. Catal. A 337 (2008) 155–162.
[48] W. Chen, W. Sheng, F. Cao, Y. Lu, Int. J. Hydrog. Energy 37 (2012) 18021–18030.
[49] J.H. Lee, D.L. Trimm, Fuel Process. Technol. 42 (1995) 339–359.
[50] A.R. Denton, N.W. Ashcroft, Phys. Rev. A: At. Opt. Phys. 43 (1991) 3161–3164.
[51] K.W. Wang, S.R. Chung, C.W. Liu, J. Phys. Chem. C 112 (2008) 10242–10246.
[52] K. Kim, N. Winograd, Chem. Phys. Lett. 30 (1975) 91–95.
[53] F.F. Tao, M. Salmeron, Science 331 (2011) 171–174.
[54] S.U. Son, Y. Jang, J. Park, H.B. Na, H.M. Park, H.J. Yun, J. Lee, T. Hyeon, J. Am. Chem. Soc. 126 (2004) 5026–5027.
[55] X. Zhang, C.S.M. Lee, D.O. Hayward, D.M.P. Mingos, Catal. Today 105 (2005) 283–294.
[56] Q.F. Zhang, X.P. Wu, G.F. Zhao, Y.K. Li, C.Z. Wang, Y. Liu, X.Q. Gong, Y. Lu, Chem. Commun. 51 (2015) 12613–12616.
[57] Y. Deng, T.G. Nevell, Faraday Discuss. 105 (1996) 33–46.
[58] A. Eyssler, A. Winkler, P. Mandaliev, P. Hug, A. Weidenkaff, D. Ferri, Appl. Catal. B 106 (2011) 494–502.
[59] C.A. Müller, M. Maciejewski, R.A. Koeppel, R. Tschan, A. Baiker, J. Phys. Chem. 100 (1996) 20006–20014.
[60] P. Gélin, L. Urfels, M. Primet, E. Tena, Catal. Today 83 (2003) 45–57.
[61] K. Fujimoto, F.H. Ribeiro, M. Avalos-Borja, E. Iglesia, J. Catal. 179 (1998) 431–442.
[62] M. Hoffmann, S. Kreft, G. Georgi, G. Fulda, M.-M. Pohl, D. Seeburg, C. Berger-Karin, E.V. Kondratenko, S. Wohlrab, Appl. Catal. B 179 (2015) 313–320.